Generation and direct measurement of giant chirp in a passively mode-locked laser

E. J. R. Kelleher,[1,*] J. C. Travers,[1] E. P. Ippen,[2] Z. Sun,[3] A. C. Ferrari,[3] S. V. Popov,[1] and J. R. Taylor[1]

[1]*Femtosecond Optics Group, Department of Physics, Imperial College London, Prince Consort Road, London SW7 2AZ, UK*

[2]*Department of Electrical Engineering and Computer Science and The Research Laboratory of Electronics, Massachusetts Institute of Technology, Cambridge, Massachusetts 02139, USA*

[3]*Department of Engineering, University of Cambridge, Cambridge CB3 0FA, UK*

**Corresponding author: edmund.kelleher08@imperial.ac.uk*

Received June 12, 2009; revised August 11, 2009; accepted September 16, 2009; posted October 15, 2009 (Doc. ID 112753); published November 11, 2009

We evaluate the shape and chirp of nanosecond pulses from a fiber laser passively mode locked with a nanotube-based saturable absorber by using a synchronously scanning streak camera and a monochromator to directly measure the pulse spectrogram. We show that the stable sech^2 output pulse possesses a predominantly linear chirp, with a residual quartic phase and low noise. Comparison with analytical mode-locking theory shows a good quantitative agreement with the master equation mode-locking model. © 2009 Optical Society of America

OCIS codes: 140.4050, 140.3510.

Recently, a new operating parameter range was reported for all-normal dispersion (ANDi [1]), passively mode-locked fiber lasers, exhibiting low repetition rates and long pulse durations [2]. Subsequently, Kobtsev *et al.* [3] and Tian *et al.* [4] demonstrated very long pulses (nanosecond scale), ultralow repetition rates, and relatively low average powers but significant pulse energies (up to 4 μJ) by passively mode locking strongly normal dispersion, ultralong cavity, Yb-based fiber lasers. Despite a peak power exceeding 1 kW in [3], no stimulated Raman scattering (SRS) was reported. Although these giant-chirp oscillators (GCOs) have been already suggested as suitable for compression (and [2] demonstrated compression in a shorter cavity), to date the nature of the chirp has not been experimentally measured and fully discussed. It is also well known that stable, low-coherence noise bursts with durations up to 10 ns and consequently high-pulse energies can be generated where nonlinear polarization evolution (NPE) is employed together with extra, normally dispersive fiber added for stability [5], and such noise bursts may be the explanation for a lack of SRS in [3]. Therefore, both coherent GCOs and noise bursts are possible with NPE, and it might be expected that similar low-coherence performance could be obtained from a GCO mode locked using some other saturable absorbing mechanism.

In this Letter we report what is, to the best of our knowledge, the first experimental measurement of the spectrogram of a nanosecond pulse duration GCO, retrieve the phase of the pulses, and discuss the degree of chirp linearity. We also show that the resulting temporal profile is clean and has a sech^2 pulse shape with low noise, through a variety of diagnostics. The dynamics of fast-saturable absorber-based mode-locking in a traveling wave resonator can be modeled using the master mode locking (MML) equation of Haus *et al.* [6], where parameters such as gain, loss, filtering, and saturable absorption are treated as perturbations to the nonlinear Schrödinger equation. We show that this well established description of a mode-locked laser has the essential features to quantitatively characterize mode locking of a GCO, even in the nanosecond regime.

The GCO is shown in Fig. 1 and detailed in [7]. The cavity consisted of a 2 m, highly Yb-doped fiber amplifier followed by a single wall carbon nanotube (SWNT)-polyvinyl alcohol (PVA) saturable absorber (transmission ~51%) [8–10], a polarization controller to initiate mode locking, a fused fiber coupler providing a 15% output, an in-line optical isolator, and a single-mode optical fiber with a length of ~1200 m. All of the cavity fiber had a dispersion coefficient of approximately –30 ps nm^{-1} km^{-1} and nonlinear coefficient of 3 W^{-1} km^{-1} at 1060 nm. Neither in-line spectral filters nor polarization selective components were used. The lasing wavelength selection results from the overlap of gain and spectral loss profiles of the laser components and the dynamic filtering of the saturable absorber. The GCO produced stable single pulses of 1.7 ns at 177 kHz repetition rate, with an energy of 0.18 nJ. The spectral FWHM of 0.49 nm was centered at 1058 nm [Fig. 2(a)], indicating strong chirp with a time-bandwidth product of 236. This is ~750 times the transform limit, assuming a sech^2 profile. Small, symmetric modulations on either side of the laser line are caused by a resonance owing to

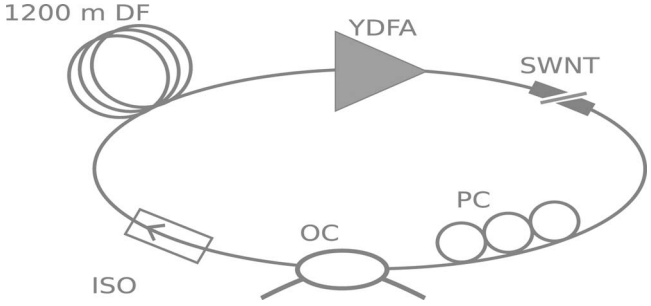

Fig. 1. GCO setup. YDFA, Yb-doped fiber amplifier; SWNT, nanotube-based saturable absorber; PC, polarization controller; OC, output coupler; ISO, isolator; DF, dispersive fiber.

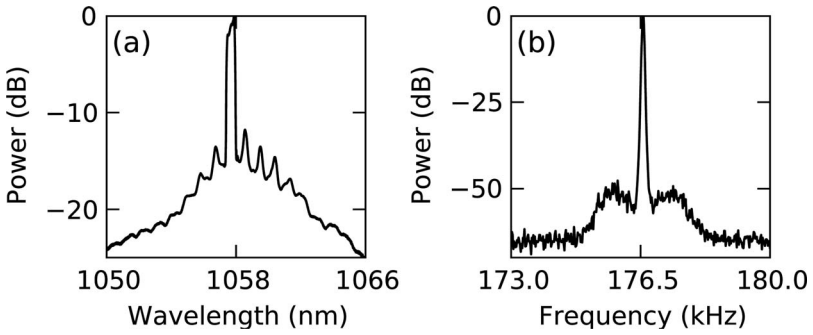

Fig. 2. (a) GCO optical and (b) rf spectrum.

the finite thickness of the nanotube film. Because of the long cavity there is time between pulses for a build up of ASE that causes a pedestal (~15 dB down from the peak) in the optical spectrum. The pulse energy is quite low in comparison to other Yb-doped fiber lasers, since a careful balance between nonlinearity and dispersion, in the very long length of fiber, and the saturable absorber action must be maintained. For our parameters this was only possible for peak powers in the subwatt regime.

The output pulse shape was measured using a synchronously scanning streak camera and is shown on a logarithmic scale in Fig. 3, along with fits to a number of pulse shapes. The sech^2 pulse shape is in agreement with analytical mode-locking theory [6,11]. The experimental setup used to measure the spectrogram is shown in Fig. 4. The output from the GCO was bulk coupled into a 1 m monochromator, incorporating a 1200 line/mm grating, with a resolution limit of ~0.05 nm at 1000 nm. The spectrally selected output of the monochromator was then focused into a synchronously scanning picosecond streak camera. The pulse intensity as a function of time was measured with the streak camera as a function of wavelength, selected by the monochromator. A typical spectrogram is shown in Fig. 5.

The spectrogram confirms a distinct chirp across the pulse. We performed a fit of the temporal phase by using the measured pulse shape (Fig. 3), adding a random initial phase and employing an iterative algorithm similar to that used in frequency resolved optical gating [12], to reproduce the measured spectrogram. The algorithm converged to the same parameters from a range of random initial phase conditions. On expanding the retrieved phase we obtain a second-order temporal phase value of $\phi_2 = 1.2 \times 10^{-4}$ ps^{-2}, a negligible third-order phase value, and a quartic phase value of $\phi_4 = -4.4 \times 10^{-12}$ ps^{-4}. These confirm the strong linear chirp of the pulse and a residual quartic phase, as seen in [11]. From the retrieved phase we can determine the expected spectral broadening of 0.40 nm, in good agreement with the measured value of 0.49 nm. If we consider only the second-order phase, then the expected broadening would be 0.57 nm and thus the quartic component acts to reduce the chirp. The transform-limited duration of the pulses is around 2–3 ps. However, it should be noted that to our knowledge it is not possible to compensate for the chirp produced from this second order phase, over several nanoseconds, with any practical compression scheme.

The spectrogram was stable over a measurement period of several hours. Tuning the transmitted wavelength of the monochromator repeatably allowed us to record the delayed pulse displayed by the streak camera. We confirmed this temporal stability with single-shot measurements on an oscilloscope. In addition, we measured the autocorrelation of the pulse over a time window of 100 ps centered on the pulse. No coherence spikes were observed, indicating the lack of noise fluctuations on picosecond and femtosecond time scales. This confirmed the temporal and spectral coherence of the pulse structure and that the nanosecond pulse did not constitute a noise

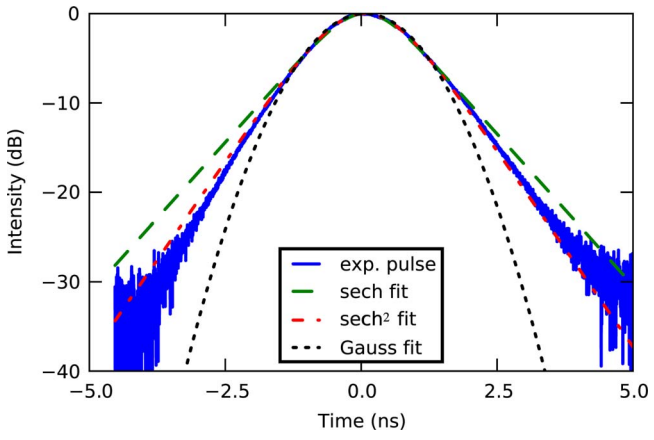

Fig. 3. (Color online) Experimentally measured pulse shape (logarithmic scale) including sech^2, sech, and Gaussian fits.

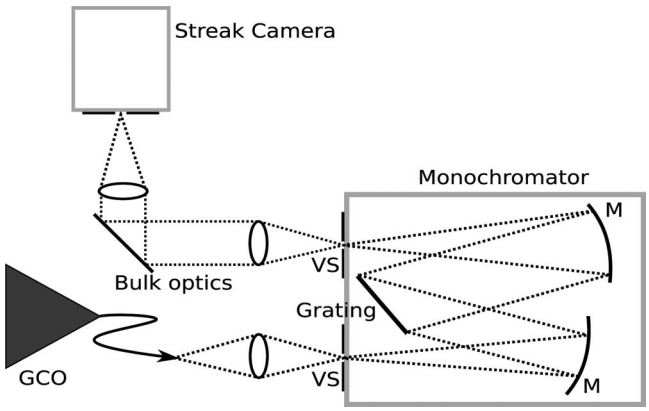

Fig. 4. Spectrogram measurement setup. GCO, giant-chirp oscillator; VS, variable slits; M, curved mirrors.

burst, typical of many long-pulse NPE-based systems [5]. To finally confirm the stability of the pulse train we measured the rf spectrum using a 2 GHz photodiode and electrical spectrum analyzer. Figure 2(b) shows that the peak to pedestal extinction was ~50 dB at a resolution of 30 Hz, comparable to many other mode-locked systems.

The experimentally measured, large linear chirp naturally arises in this mode-locking regime owing to the balance between nonlinearity, dispersion, and saturable absorption [2,6,11]. The analytical theory first developed in [6] and studied recently in [11] was used to generate a spectrogram for our pulse parameter regime. Although the inclusion of a quintic loss term has improved the robustness of the MML model and helped stabilize solutions to the governing equation by moderating the growth of the nonlinear gain term [13], we find reasonable quantitative agreement using the simple cubic, complex Ginzburg–Landau (MML) equation, even in the nanosecond regime. We used the following best-estimate values in the model: the second derivative of the propagation constant was $0.018\ \mathrm{ps}^2\ \mathrm{m}^{-1}$; the nonlinear parameter was $0.0035\ \mathrm{W}^{-1}\ \mathrm{m}^{-1}$; the resonator length was 1200 m; the central wavelength was 1057.64 nm; the gain bandwidth was 20 nm; the net system gain (or loss) was 11 dB; the minimum intracavity pulse energy was 500 pJ; and the saturable absorption coefficient $\gamma=0.035$ was tuned to give the best quantitative agreement with the measured chirp value. The theoretical spectrogram is shown in Fig. 6 and exhibits very similar structure to our measured spectrogram. The calculated phase expansion indicates a second-order temporal phase value of $\phi_2=9.5\times10^{-5}\ \mathrm{ps}^{-2}$, a negligible third-order phase value and a quartic phase value of $\phi_4=-2.2\times10^{-12}\ \mathrm{ps}^{-4}$, all of which are in very close agreement to the values extracted from our experimental spectrogram, confirming that the model incorporates all the essential features to describe this nanosecond-pulse GCO. Given that this analytical model does not include any interpulse jitter or fluctuations, the agreement with experiment indicates that our measured pulses are also not broadened by such a process, as confirmed by the oscilloscope, rf spectrum, and autocorrelation measurements discussed above.

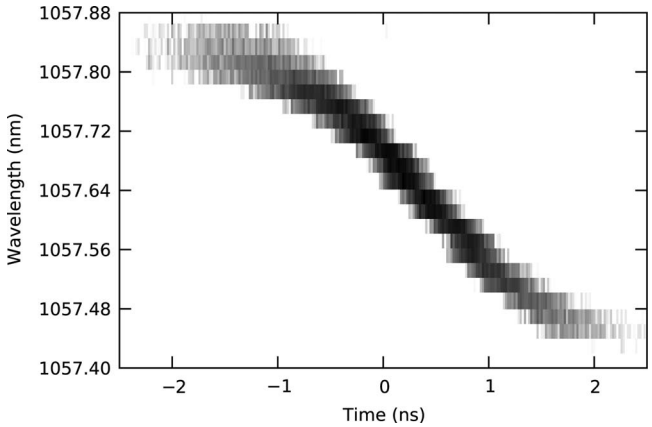

Fig. 5. Measured spectrogram. The dynamic range is 15 dB.

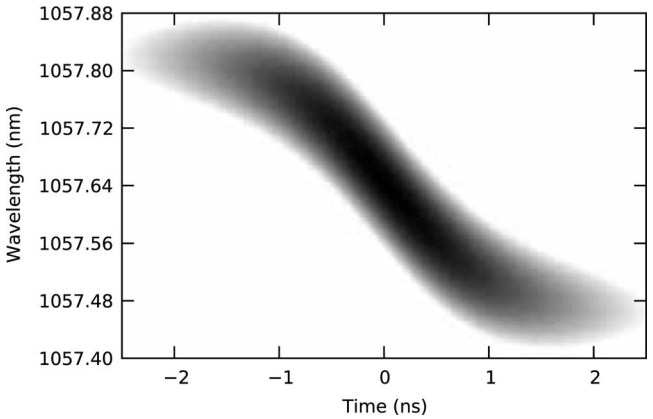

Fig. 6. Simulated spectrogram. The dynamic range is 15 dB.

In conclusion, our measurements show that the pulses from such GCOs exhibit a clean temporal profile, with no noise structure, and the nature of the chirp is linear with a residual quartic phase in excellent agreement with analytical theory.

FOG is supported by the UK Engineering and Physical Sciences Research Council (EPSRC) and Royal Society. S. V. Popov is a Royal Society Industry Fellow, J. R. Taylor is a Royal Society Wolfson Research Merit Award holder, and E. P. Ippen was supported by an EPSRC visiting fellowship. Z. Sun and A. C. Ferrari acknowledge funding from the Royal Society Brian Mercer Award for Innovation, the ERC grant NANOPOTS, and EPSRC grant EP/GO30480/1.

References

1. A. Chong, W. H. Renninger, and F. W. Wise, Opt. Lett. **32**, 2408 (2007).
2. W. H. Renninger, A. Chong, and F. W. Wise, Opt. Lett. **33**, 3025 (2008).
3. S. Kobtsev, S. Kukarin, and Y. Fedotov, Opt. Express **16**, 21,936 (2008).
4. X. Tian, M. Tang, P. P. Shum, Y. Gong, C. Lin, S. Fu, and T. Zhang, Opt. Lett. **34**, 1432 (2009).
5. M. Horowitz, Y. Barad, and Y. Silberberg, Opt. Lett. **22**, 799 (1997).
6. H. A. Haus, J. G. Fujimoto, and E. P. Ippen, J. Opt. Soc. Am. B **8**, 2068 (1991).
7. E. J. R. Kelleher, J. C. Travers, Z. Sun, A. C. Rozhin, A. G. Ferrari, S. V. Popov, and J. R. Taylor, Appl. Phys. Lett. **95**, 111108 (2009).
8. V. Scardaci, Z. Sun, F. Wang, A. G. Rozhin, T. Hasan, F. Hennrich, I. H. White, W. I. Milne, and A. C. Ferrari, Adv. Mater. **20**, 4040 (2008).
9. T. Hasan, Z. Sun, F. Wang, F. Bonaccorso, P. H. Tan, A. G. Rozhin, and A. C. Ferrari, Adv. Mater. **21**, 3874 (2009).
10. F. Wang, A. G. Rozhin, V. Scardaci, Z. Sun, F. Hennrich, I. H. White, W. I. Milne, and A. C. Ferrari, Nat. Nanotechnol. **3**, 738 (2008).
11. W. H. Renninger, A. Chong, and F. W. Wise, Phys. Rev. A **77**, 023814 (2008).
12. R. Trebino, K. W. DeLong, D. N. Fittinghoff, J. N. Sweetser, M. A. Krumbügel, B. A. Richman, and D. J. Kane, Rev. Sci. Instrum. **68**, 3277 (1997).
13. B. G. Bale and J. N. Kutz, J. Opt. Soc. Am. B **25**, 1193 (2008).